Asymmetric protonation of glutamate residues drives a preferred transport pathway in EmrE

Jianping Li[a,1], Ampon Sae Her[a,1], and Nathaniel J. Traaseth[a,2]

[a]Department of Chemistry, New York University, New York, NY 10003

Edited by Adriaan Bax, NIH, Bethesda, MD, and approved August 20, 2021 (received for review June 10, 2021)

EmrE is an *Escherichia coli* multidrug efflux pump and member of the small multidrug resistance (SMR) family that transports drugs as a homodimer by harnessing energy from the proton motive force. SMR family transporters contain a conserved glutamate residue in transmembrane 1 (Glu14 in EmrE) that is required for binding protons and drugs. Yet the mechanism underlying proton-coupled transport by the two glutamate residues in the dimer remains unresolved. Here, we used NMR spectroscopy to determine acid dissociation constants (pK_a) for wild-type EmrE and heterodimers containing one or two Glu14 residues in the dimer. For wild-type EmrE, we measured chemical shifts of the carboxyl side chain of Glu14 using solid-state NMR in lipid bilayers and obtained unambiguous evidence on the existence of asymmetric protonation states. Subsequent measurements of pK_a values for heterodimers with a single Glu14 residue showed no significant differences from heterodimers with two Glu14 residues, supporting a model where the two Glu14 residues have independent pK_a values and are not electrostatically coupled. These insights support a transport pathway with well-defined protonation states in each monomer of the dimer, including a preferred cytoplasmic-facing state where Glu14 is deprotonated in monomer A and protonated in monomer B under pH conditions in the cytoplasm of *E. coli*. Our findings also lead to a model, hop-free exchange, which proposes how exchangers with conformation-dependent pK_a values reduce proton leakage. This model is relevant to the SMR family and transporters comprised of inverted repeat domains.

EmrE | transport mechanisms | multidrug resistance | protein dynamics | small multidrug resistance family

Antibiotic resistance arises from multiple molecular mechanisms, including the enzymatic breakdown of drugs, mutations of target proteins, reduced drug influx, and the activation of efflux pumps (1). The efflux mechanism by membrane protein transporters is one of the broadest resistance mechanisms that requires active transport to reduce the internal drug concentration. Four out of five drug efflux families are secondary active transporters and share the following features: i) broad binding specificity to toxic compounds including antibiotics, antiseptics, and cationic dyes, ii) undergo conformational exchange to catalyze the substrate transport across the membrane, and iii) contain essential anionic residues needed for binding protons and/or substrates.

Escherichia coli EmrE from the SMR family has served as a model of drug transport since it contains the minimal required complexity (110 residues) and shares each of the features found in other drug transporters. Namely, it forms an antiparallel homodimer that is required for drug efflux (2–6), it undergoes conformational exchange needed for drug transport (7, 8), and it contains a conserved anionic residue at Glu14 in each monomer of the dimer that is essential for antiport of protons (3, 5, 6, 9–11). While these studies provided insight into features of EmrE needed for drug efflux, key questions remain about the ion-coupled transport mechanism. Specifically, it is unclear whether the two Glu14 residues can exhibit differential protonation states in a lipid bilayer environment and whether deprotonation at one monomer influences the acid dissociation constant (pK_a) of the other monomer in the dimer (i.e., electrostatic coupling).

Here, we used NMR spectroscopy and pH titrations to quantify chemical shift perturbations of Glu14 and surrounding residues in a monomer specific manner within the EmrE dimer. These measurements allowed us to derive monomer specific changes for accurately assessing the Glu14 protonation states within EmrE and determine that the two Glu14 residues in the dimer have independent pK_a values. Using our findings, we propose a transport model for EmrE with Glu14 protonation states specified for each monomer and discuss the implications of this model for minimizing proton leakage while achieving efficient proton-coupled drug efflux.

Results

Asymmetric Glu14 Protonation in EmrE Determined Using Solid-State NMR Spectroscopy. We aimed to determine protonation states of Glu14 in EmrE using NMR spectroscopy by directly detecting the ^{13}C chemical shift of the carboxyl carbon since this observable strongly correlates with the protonation state (12). Uniformly $^{13}C/^{15}N$ labeled, wild-type EmrE was reconstituted into lipid bilayers comprised of diether lipids (*O*-14:0-*O*-PC) to ensure stability throughout NMR data collection at different pH values. Double-quantum single-quantum rotational-echo double-resonance (DQSQ-REDOR) (13) magic-angle-spinning spectra were acquired on EmrE samples at pH values of 5.0, 8.0, and 10.0 (Fig. 1*A*). The three anionic residues in EmrE (Glu14, Glu25, Asp84) were clearly resolved in the spectra at each pH value, with assignments confirmed using mutagenesis and $^{13}C/^{13}C$ correlation experiments (14) (*SI Appendix*, Fig. S1). Of these residues, only Glu14 experienced a chemical shift perturbation from pH 5.0 to 10.0. The chemical shift at pH 5.0 was 176.0 ppm (Fig. 1*A*, *Top*), while its

Significance

EmrE is a proton-coupled efflux pump that confers multidrug resistance to *Escherichia coli*. Here, we probed the electrostatic environment surrounding each essential Glu14 residue in the EmrE dimer by determining monomer specific pK_a values using NMR spectroscopy. We discovered that acid/base chemistry at one of the two Glu14 residues in the homodimer potentiates a global conformational change within EmrE. Our findings revealed that asymmetric protonation states of EmrE leads to a preferred pathway of substrate transport. These insights led to a model to explain how EmrE accomplishes proton-coupled transport without leaking protons. Since the overall structure of EmrE resembles those of other transporters containing inverted repeat domains, our findings have application to other secondary active transporters.

Author contributions: J.L., A.S.H., and N.J.T. designed research; J.L. and A.S.H. performed research; J.L., A.S.H., and N.J.T. analyzed data; and J.L., A.S.H., and N.J.T. wrote the paper.

The authors declare no competing interest.

This article is a PNAS Direct Submission.

[1]J.L. and A.S.H. contributed equally to this work.

[2]To whom correspondence may be addressed. Email: traaseth@nyu.edu.

This article contains supporting information online at https://www.pnas.org/lookup/suppl/doi:10.1073/pnas.2110790118/-/DCSupplemental.

Published October 4, 2021.

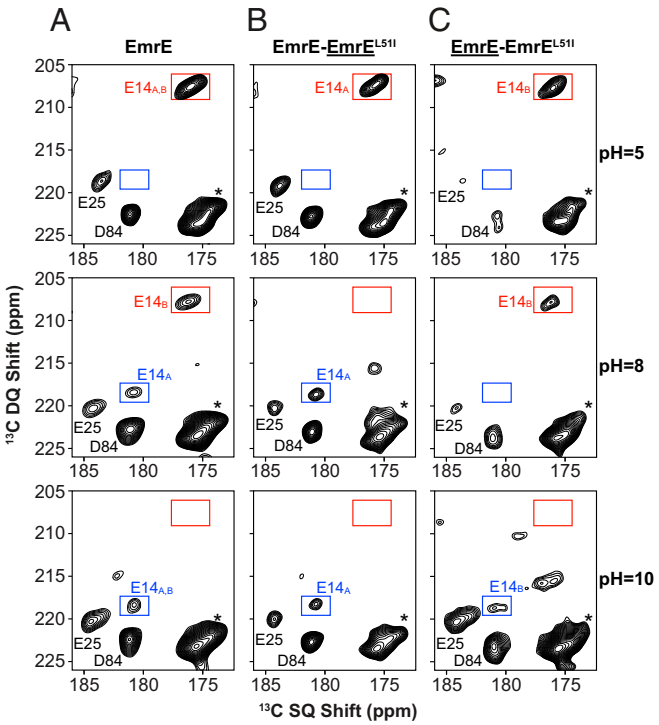

Fig. 1. Detection of Glu14 chemical shifts in EmrE using solid-state NMR spectroscopy in lipid bilayers. (*A*) DQSQ-REDOR spectra of uniformly $^{13}C/^{15}N$ labeled EmrE. (*B*) DQSQ-REDOR spectra of heterodimers composed of $^{13}C/^{15}N$ labeled EmrE^{L51I} and natural abundance EmrE. (*C*) DQSQ-REDOR spectra of heterodimers composed of $^{13}C/^{15}N$ labeled EmrE and natural abundance EmrE^{L51I}. Each spectrum was collected at pH values of 5.0 (*top row*), 8.0 (*middle row*), and 10.0 (*bottom row*). The underlined protein indicates the isotopically enriched monomer in the heterodimer. The peak positions of protonated and deprotonated Glu14 residues are shown in red and blue boxes, respectively. Asterisks denote residual signals from backbone glycine residues.

chemical shift at pH 10.0 was 180.8 ppm (Fig. 1*A*, *Bottom*). The protonated chemical shift of Glu14 was ∼8 ppm upfield from the solvent accessible Glu25 residue within EmrE, which likely reflects the hydrophobic environment surrounding this side chain within the substrate binding pocket. However, the difference of 4.8 ppm between chemical shifts at pH values of 5.0 and 10.0 matches with the expected span between protonated and deprotonated side chains of glutamate residues (12). Therefore, we conclude that Glu14 residues are predominantly proton-bound at pH 5.0 ($E_A{}^H$-$E_B{}^H$) and deprotonated at pH 10.0 ($E_A{}^-$-$E_B{}^-$), where E_A and E_B correspond to each monomer of the EmrE crystal structure bound to tetraphenylphosphonium (15). Note that the association of monomers in the crystal structure with NMR experiments is based on the agreement of helical tilt angles estimated from the structure and those determined using oriented sample solid-state NMR spectroscopy (16–19).

In contrast to NMR spectra at pH 5.0 or 10.0, we observed two peaks for Glu14 of EmrE in the DQSQ-REDOR spectrum at pH 8.0 that matched the chemical shifts of the protonated and deprotonated species (Fig. 1*A*, *Middle*). This result suggested the two Glu14 residues had asymmetric protonation states in the dimer. To test this hypothesis, we prepared heterodimer samples by mixing wild-type EmrE with the L51I mutant (EmrE^{L51I}) (19). Such samples result in a preferred conformational equilibrium where wild-type EmrE occupies monomer B position in the heterodimer and EmrE^{L51I} occupies monomer A position (*SI Appendix*, Fig. S2). DQSQ-REDOR spectra of $^{13}C/^{15}N$ labeled EmrE mixed with unlabeled EmrE^{L51I} and the opposite isotopic labeling scheme were acquired at pH values of 5.0, 8.0, and 10.0 (Fig. 1 *B* and *C*). Unlike the two peaks observed for Glu14 in the wild-type spectrum at pH 8.0, each heterodimer sample displayed a single peak for Glu14 at pH 8.0. Namely, the carboxyl chemical shift for Glu14 of monomer B (EmrE) in the heterodimer appeared at 176.2 ppm, indicating a protonated state (Fig. 1*C*, *Middle*), while Glu14 of monomer A (EmrE^{L51I}) appeared at 180.8 ppm, indicating a deprotonated state (Fig. 1*B*, *Middle*). As a control, we observed Glu14 carboxyl chemical shifts at pH values of 5.0 and 10.0 for each heterodimer sample that were in agreement with those observed in the corresponding wild-type EmrE spectrum. From these data, we conclude EmrE contains Glu14 residues that are asymmetrically protonated in lipid bilayers, where Glu14 in monomer A is more acidic ($5.0 < pK_a < 8.0$) than that of monomer B ($8.0 < pK_a < 10.0$).

pK_a Values Determined Using Solution NMR Spectroscopy. To determine pK_a values in a monomer specific manner, we used solution NMR spectroscopy in dimyristoyl-sn-glycero-3-phosphocholine/dihexanoyl-sn-glycero-3-phosphocholine (DMPC/DHPC) isotropic bicelles since it was more robust for collecting several data sets over a range of pH values. We employed our heterodimer technology involving EmrE and EmrE^{L51I} and performed pH titrations on samples where only one protein was isotopically enriched. $^1H/^{15}N$ transverse relaxation optimized spectroscopy (TROSY) spectra showed that the conformational equilibrium of the EmrE-EmrE^{L51I} heterodimer was maintained from pH 5.0 to 10.0 and at a temperature of 37 °C needed for collecting high-quality NMR spectra (*SI Appendix*, Figs. S3 and S4). The change in conformational equilibrium induced by the L51I mutation in the EmrE-EmrE^{L51I} heterodimer corresponds to a free energy of ∼1.8 kcal/mol (19). Note that the heterodimer approach overcame the limitation of pH dependent conformational exchange previously observed in wild-type EmrE (8, 20), which complicates spectral analysis and does not afford monomer specific chemical shift perturbations (CSPs) to be quantified (8, 21).

CSPs in monomers A and B were quantified from $^1H/^{15}N$ TROSY spectra for several residues within the EmrE-EmrE^{L51I} heterodimer. Monomer A peaks displayed several large CSPs, including for residues $Gly9_A$ and $Gly17_A$ that are close in proximity to $Glu14_A$ (Fig. 2*A*, *SI Appendix*, Fig. S4*A*). Monomer B peaks also displayed large CSPs for $Gly9_B$ and $Gly17_B$ that are near $Glu14_B$ (Fig. 2*B*, *SI Appendix*, Fig. S4*B*). Notably, we observed a striking nonlinear CSP for $Gly17_B$ (Fig. 2*B*), indicative of a multistep process. This observation suggested that $Gly17_B$ was sensitive to acid/base chemistry at both Glu14 residues in the dimer, consistent with the asymmetric Glu14 protonation state observed in solid-state NMR experiments (Fig. 1). We globally fit CSPs in proximity to Glu14 using a modified Henderson–Hasselbalch equation with two pK_a values (Eq. **1**), yielding values of 7.2 ± 0.1 and 8.4 ± 0.2 (Fig. 2 *C* and *D*). These solution NMR results support the conclusion that under a physiologically relevant temperature of 37 °C and a cytoplasmic pH of 7.5, the preferred state of EmrE is bound to one proton in monomer B ($E_A{}^-$-$E_B{}^H$). Our observations are in agreement with pK_a values reported by Morrison et al. (21) (7.0 ± 0.1 and 8.2 ± 0.3) and the ΔpK_a computed by Vermaas et al. (22) ($\Delta pK_a = 1.08$); however, our findings contrast with the pK_a values reported by Ovchinnikov et al. (8.80 to 9.32 and 10.45 to 11.38) (23).

Deprotonation of Glu14 in Monomer A Triggers a Global Conformational Change. In pH titration experiments of the EmrE-EmrE^{L51I} heterodimer, most residues displayed CSPs that coincided with the more acidic pK_a value, suggesting $Glu14_A$ deprotonation induced the more significant conformational change within the dimer. To test this hypothesis, we prepared a heterodimer with a single Glu14 residue in the dimer by mixing EmrE with the E14Q mutation of EmrE (EmrE^{E14Q}). Similar to other heterodimer samples, isotopically enriched EmrE or EmrE^{E14Q} was mixed with the partner

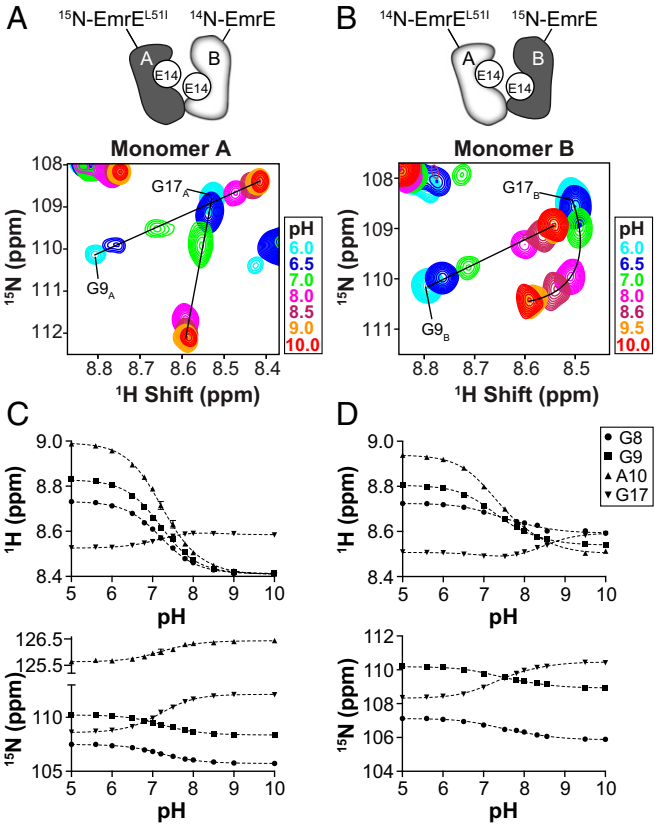

Fig. 2. Determination of pK_a values for Glu14 residues in the EmrE-EmrE^{L51I} heterodimer using solution NMR spectroscopy. (*A*) ^{1}H/^{15}N TROSY spectra at the indicated pH values for heterodimers composed of isotopically enriched EmrE^{L51I} and natural abundance EmrE. (*B*) ^{1}H/^{15}N TROSY spectra at the indicated pH values for heterodimers composed of isotopically enriched EmrE and natural abundance EmrE^{L51I}. (*C* and *D*) Chemical shifts as a function of pH for (*C*) monomer A and (*D*) monomer B. The dotted line is the global fit to the two-pK_a model in Eq. 1.

protein at natural abundance, and ^{1}H/^{15}N TROSY spectra were acquired at several pH values (Fig. 3 *A* and *B*, *SI Appendix*, Fig. S4 *C* and *D*). For each pH value, isotopically enriched EmrE in the heterodimer displayed more intense monomer A signals, while isotopically enriched EmrE^{E14Q} displayed more intense monomer B signals. Using monomer A and B peak intensities, we estimated free energies of the conformational equilibria at ~3.5 kcal/mol for pH 9.5 and ~0.6 kcal/mol for pH 6.2 (*Materials and Methods*). The larger free energy difference at the basic pH value indicated a greater preference for the deprotonated Glu14 in the heterodimer to occupy the monomer A position.

Several residues in monomers A and B of the EmrE-EmrE^{E14Q} heterodimer incurred large CSPs as a function of pH (Fig. 3 *A* and *B*). Residues in the vicinity of monomer A (Gly9$_A$, Ala10$_A$, Gly17$_A$) displayed nearly identical CSPs as the EmrE-EmrE^{L51I} heterodimer, while residues near Glu14 in monomer B (Gly9$_B$, Ala10$_B$, Gly17$_B$) also displayed significant CSPs. However, we did not observe nonlinear CSPs for monomer B residues like in the EmrE-EmrE^{L51I} heterodimer experiment. Notably, Gly17$_B$ showed a linear CSP in EmrE-EmrE^{E14Q} pH titrations (Fig. 3*B*), which contrasted with the striking nonlinear CSP observed in the EmrE-EmrE^{L51I} titration (Fig. 2*B*). A single pK_a value adequately fit all CSP data for EmrE-EmrE^{E14Q}, in agreement with the single Glu14 in the dimer (Fig. 3 *C* and *D*). These fits yielded a pK_a value of 7.2 ± 0.1, which was in quantitative agreement with the more acidic pK_a value determined from EmrE-EmrE^{L51I} heterodimer experiments.

We also compared chemical shift changes between pH 5.0 and 10.0 for residues in the heterodimers with one Glu14 (EmrE-EmrE^{E14Q}) or two Glu14 residues (EmrE-EmrE^{L51I}) (Fig. 4 *A* and *B*). The correlation plots displayed slopes of 0.90 ± 0.06 for monomer A residues and 0.57 ± 0.08 for monomer B residues (Fig. 4*C*). The slope close to unity for monomer A suggested a strong similarity of conformational changes in monomer A for dimers with one or two protonatable Glu14 residues (i.e., EmrE-EmrE^{L51I}). A larger deviation from unity was observed for the slopes of monomer B peaks and indicated deprotonation of Glu14^B was responsible for additional CSPs within monomer B, such as Ala10$_B$ and Gly67$_B$, relative to those in the EmrE-EmrE^{L51I} heterodimer (Fig. 4*B*). However, CSPs plotted onto the structure of EmrE showed very similar profiles for EmrE-EmrE^{L51I} and EmrE-EmrE^{E14Q} heterodimers, albeit with a few small differences around Glu14$_B$ (Fig. 4*D*). Overall, these results support the conclusion that deprotonation of Glu14 within monomer A serves as the primary site responsible for triggering a global conformational change in the EmrE dimer. Such a change may involve differences in solvent accessibility of the substrate binding site, which has been observed in molecular dynamics simulations (22).

Glu14 Residues Are Not Electrostatically Coupled. Two pK_a values raised the question whether the Glu14 residues in the dimer are electrostatically coupled (21). If coupling existed, deprotonation at one Glu14 residue may increase or decrease the apparent pK_a value of the other Glu14 site. By contrast, if Glu14 sites were

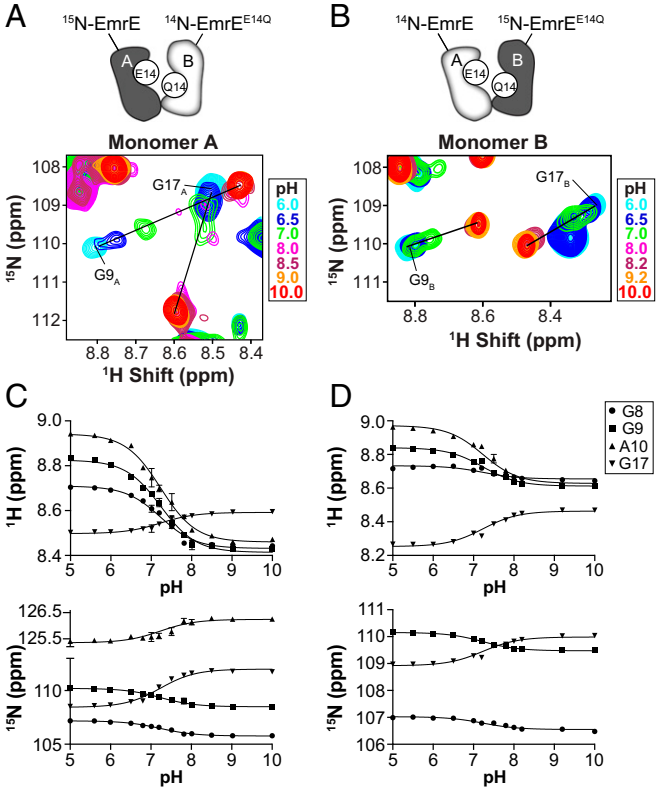

Fig. 3. Determination of the pK_a value for Glu14 in monomer A of the EmrE-EmrE^{E14Q} heterodimer using solution NMR spectroscopy. (*A*) ^{1}H/^{15}N TROSY spectra at the indicated pH values for heterodimers composed of isotopically enriched EmrE and natural abundance EmrE^{E14Q}. (*B*) ^{1}H/^{15}N TROSY spectra at the indicated pH values for heterodimers composed of isotopically enriched EmrE^{E14Q} and natural abundance EmrE. (*C* and *D*) Chemical shifts as a function of pH for (*C*) monomer A and (*D*) monomer B. The dotted line is the global fit to the one-pKa model in Eq. 2.

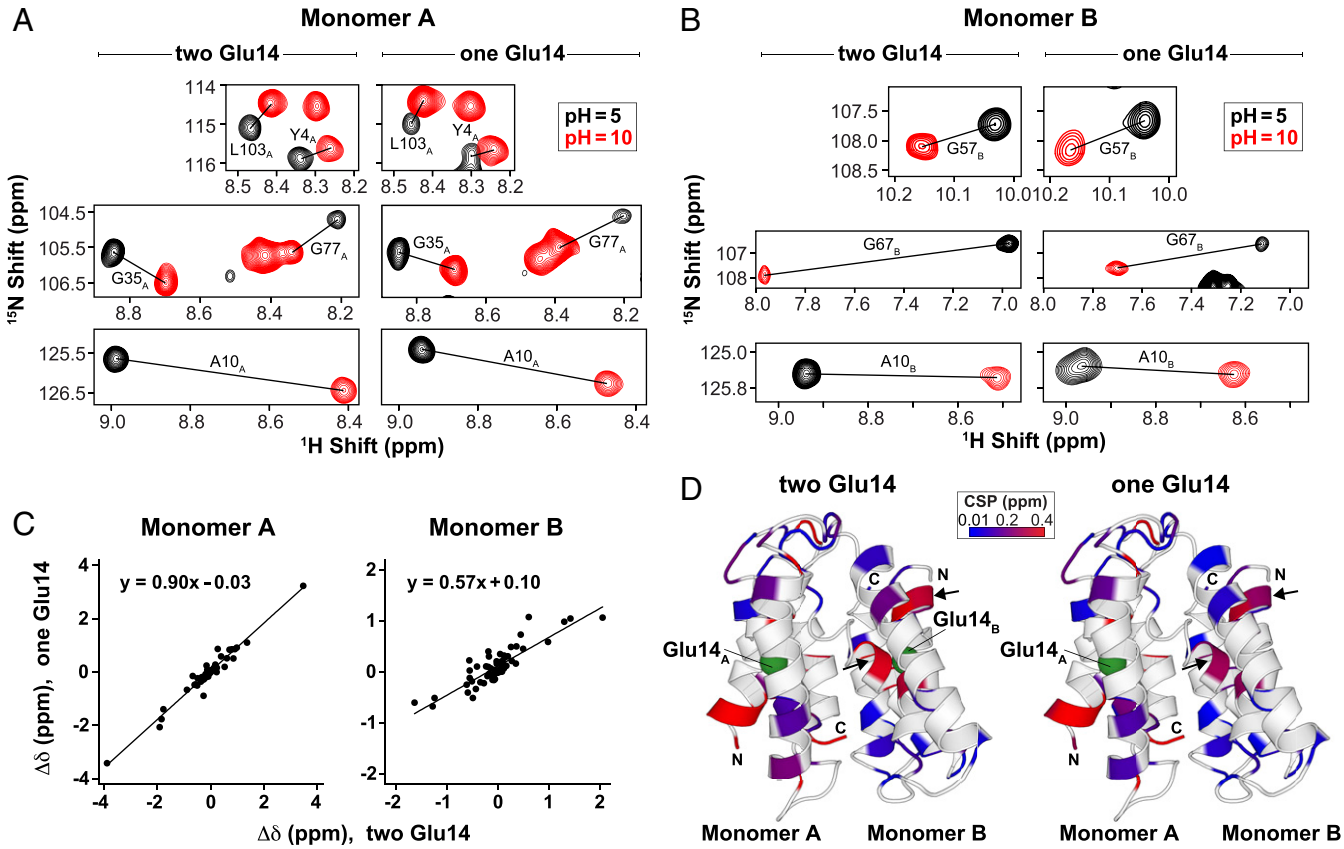

Fig. 4. Chemical shift comparison for heterodimers comprised of one or two Glu14 residues. (*A*) ^{1}H/^{15}N TROSY spectra of heterodimers at pH 5.0 (black) and pH 10.0 (red) for monomer A residues in EmrE-EmrE^{L51I} (*left*, "two Glu14") and EmrE-EmrE^{E14Q} (*right*, "one Glu14"). (*B*) ^{1}H/^{15}N TROSY spectra of heterodimers at pH 5.0 (black) and pH 10.0 (red) for monomer B residues in EmrE-EmrE^{L51I} (*left*, "two Glu14") and EmrE-EmrE^{E14Q} (*right*, "one Glu14"). (*C*) Correlation plots of the chemical shift difference (Δδ) between pH 5.0 and pH 10.0 for residues in monomer A (*left*) and monomer B (*right*). The *y*-axis name, "two Glu14," corresponds to the EmrE-EmrE^{L51I} heterodimer, while the x-axis name, "one Glu14," corresponds to the EmrE-EmrE^{E14Q} heterodimer. (*D*) Combined ^{1}H/^{15}N CSPs between pH values of 5.0 and 10.0 plotted onto the EmrE structure [Protein Data Bank: 3B5D (15)] for data derived from the EmrE-EmrE^{L51I} ("two Glu14") and EmrE-EmrE^{E14Q} ("one Glu14") heterodimers. The color range from blue to red corresponds to the smallest to largest CSPs, respectively. Arrows highlight differences in the CSP profiles.

uncoupled, each Glu14 would have an independent pK_a value that would not depend on the protonation state of the other. Heterodimer experiments in Figs. 2 and 3 provided clues about the coupling mechanism since the pK_a value of 7.2 for Glu14$_A$ of EmrE-EmrE^{E14Q} matched the more acidic pK_a value in the EmrE heterodimer with two Glu14 residues (8).

We hypothesized that a heterodimer of EmrE and the double mutant EmrE$^{E14Q,\ L51I}$ would allow us to estimate the pK_a value for Glu14$_B$ in the absence of a protonatable site within monomer A (Fig. 5*A*). Hence, we mixed isotopically enriched EmrE with excess EmrE$^{E14Q,\ L51I}$ at natural abundance and acquired ^{1}H/^{15}N TROSY spectra at different pH values (Fig. 5 *B* and *C*; *SI Appendix*, Fig. S5). We observed intense monomer B peaks at pH < 8.5 and intense monomer A peaks at pH ≥ 8.5, supporting a change in the conformational equilibrium around this pH value. These data indicated that the L51I mutation of EmrE$^{E14Q,\ L51I}$ influenced the equilibrium when Glu14 in the EmrE monomer was protonated, favoring EmrE as monomer B in the heterodimer. Conversely, deprotonated Glu14 in the EmrE monomer elicited a stronger preference, favoring EmrE as monomer A in the heterodimer. Thus, the pK_a value could be estimated at the pH value where monomers A and B were equally populated. In addition to these intensity changes, we observed CSPs from pH 6.3 to 8.5 within monomer B peaks of EmrE in the heterodimer (Fig. 5 *B* and *C*). These perturbations were consistent with a two-step process involving a fast step followed by a slow step, where the fast step corresponded to proton binding/unbinding within monomer B and the slow step to conformational exchange to monomer A in the heterodimer (Fig. 5*A*).

The population of EmrE in monomer B (p_B) was calculated by analyzing the intensities of monomer A and B peaks for residues in proximity to Glu14 as a function of pH (Fig. 5*D*). These populations were fitted to a modified Henderson–Hasselbalch equation and gave a pK_a value of 8.3 ± 0.1 for Glu14$_B$. This pK_a value was in good agreement with the more basic pK_a value (8.4 ± 0.2) observed in EmrE-EmrE^{L51I} experiments. Hence, pK_a values determined for Glu14$_A$ and Glu14$_B$ in heterodimers containing a single Glu14 residue were consistent with the two pK_a values observed for heterodimers containing two Glu14 residues. This observation indicates the presence of independent pK_a values and the absence of electrostatic coupling. These results also imply that Glu14 residues are somewhat distant inside the substrate binding pocket or that the presence of water screens the charges on the glutamate residues (22, 23). Although there is no experimental structure of proton-bound EmrE (E_A^H-E_B^H), molecular dynamics simulations performed on this state displayed an average distance between the two Glu14 residues of 13.6 Å (*SI Appendix*, Fig. S6) (22). Such a distance exceeds those found in typical electrostatic interactions (24, 25) and supports experimental NMR measurements indicating the absence of electrostatic coupling between Glu14 residues. Finally, these results underscore that the two pK_a values arise from

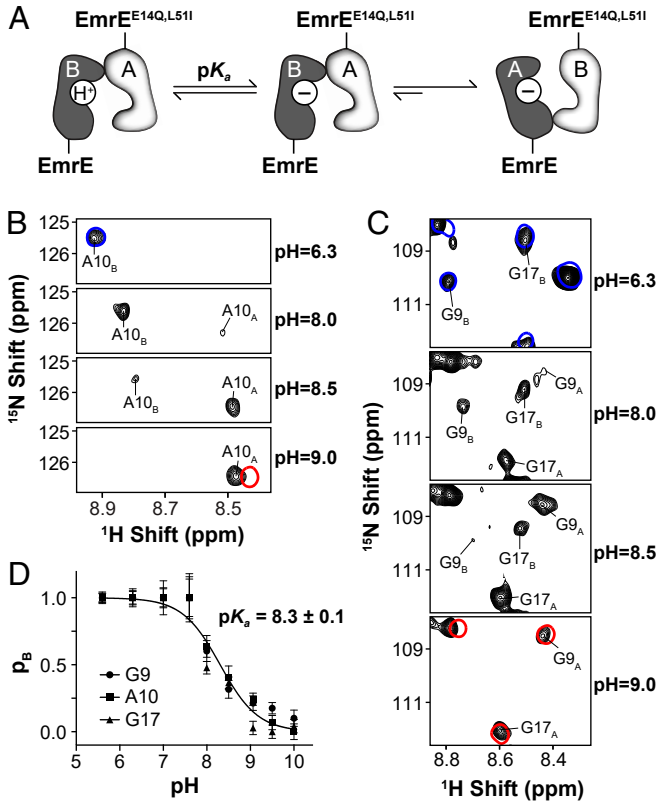

Fig. 5. Determination of the pK_a value for Glu14 in monomer B of the EmrE-EmrE^{E14Q,L51I} heterodimer using solution NMR spectroscopy. (*A*) Cartoon representation of EmrE-EmrE^{E14Q,L51I} heterodimer experiments where "H$^+$" and "−" refer to protonated and deprotonated Glu14, respectively. (*B* and *C*) ^{1}H/^{15}N TROSY spectra of isotopically enriched EmrE in the EmrE-EmrE$^{E14Q,\ L51I}$ heterodimer (black). The superimposed spectra in blue and red correspond to monomer B peaks at pH 6.3 (blue) and monomer A peaks at pH 9.0 (red) as measured from the EmrE-EmrE^{L51I} heterodimer sample. (*D*) Population of monomer B (p_B) in the EmrE-EmrE^{E14Q,L51I} heterodimer calculated by dividing the intensity of monomer B peaks by the sum of intensities of monomer A and B peaks. The fitted line indicates the pK_a value for Glu14 of monomer B.

different conformations in the asymmetric EmrE dimer and not from electrostatic coupling.

Discussion

EmrE's transport cycle requires the presence of proton and drug bound forms and conformational exchange between inward-open and outward-open states. Here, we determined E_A^--E_B^H to be the most populated conformer of drug-free EmrE under pH conditions found in the cytoplasm of *E. coli* (pH ∼7.5). We hypothesize this state plays a central role in the transport cycle since it can bind a drug substrate, bind to a proton at Glu14$_A$, or undergo deprotonation at Glu14$_B$. Unlike the other drug-free states of EmrE (E_A^H-E_B^H and E_A^--E_B^-), E_A^--E_B^H has different protonation states at the two Glu14 residues in the dimer. Hence, if exchange occurred between inward-open and outward-open states of E_A^--E_B^H, the proton would transfer from one monomer to the other during the conformational change (Fig. 6*A*). As a result, this proton hopping mechanism would rapidly dissipate a pH gradient across a membrane. Notably, the conformational exchange rate accompanying proton hopping was set to 100 s^{-1}, which is ∼14-fold faster than conformational exchange when EmrE is drug bound (7.3 s^{-1}) (9). This indicates that proton hopping would not be the rate limiting step in the transport cycle. This mechanism is a central feature of the free exchange model of EmrE and simulations of the transport cycle required the inclusion of fixed concentrations of protons on both sides of the membrane to prevent proton leakage predicted by the model (9). Yet, EmrE and other SMR family members do not leak protons (9, 26, 27), suggesting conformational exchange occurs when EmrE is bound to a drug substrate or both protons at Glu14. Furthermore, independent pK_a values measured for Glu14 residues in this work and the relatively long distance between Glu14 residues in molecular dynamics simulations (22, 23) suggests no significant electrostatic coupling between the two anionic residues within the substrate binding pocket, which would be expected from an efficient proton transfer process. Taken together, these observations imply that an alternative mechanism is needed to explain the ion-coupled transport cycle for EmrE.

Here, we propose a hop-free model where conformational exchange and proton transfer do not occur simultaneously (Fig. 6*B*). This mechanism is consistent with NMR observations that detected no electrostatic coupling between the Glu14 residues. In the hop-free model, inward-open E_A^--E_B^H exchanges with outward-open E_A^H-E_B^- and outward-open E_A^--E_B^H exchanges with inward-open E_A^H-E_B^-. In contrast to exchange in the proton hopping model, the free energies of exchanging states are different in our model. Indeed, conformational exchange of E_A^--E_B^H to E_A^H-E_B^- is strongly disfavored since the relative free energy of E_A^H-E_B^- is higher than E_A^--E_B^H. We estimated this free energy difference at ∼2.9 kcal/mol using EmrE-EmrE^{E14Q} heterodimer experiments (*Materials and Methods*), which reduces the probability of exchange and therefore proton leakage.

The hop-free mechanism is consistent with two key observations in the literature. First, growth inhibition assays in *E. coli* showed that heterodimers of EmrE-EmrE^{E14Q} do not confer drug resistance (19, 28). We found that EmrE-EmrE^{E14Q} displayed a biased conformational equilibrium that would halt the transport cycle and account for the ablated phenotype. This explanation is consistent with the correlation we established between the inward-open/outward-open conformational equilibrium and reduced growth inhibition in *E. coli* (19). Hence, the hop-free model is not in conflict with the EmrE-EmrE^{E14Q} growth inhibition data but rather explains these observations with a biased conformational equilibrium.

Second, conformational exchange experiments performed on wild-type EmrE showed decreased exchange rates from acidic to basic pH values (8). These data suggest significantly slower exchange for E_A^--E_B^H and E_A^--E_B^- relative to E_A^H-E_B^H. However, due to the relatively small difference in pK_a values for the two Glu14 residues, it is not possible to directly measure the exchange rate for E_A^--E_B^H in the absence of contributions from E_A^--E_B^- or E_A^H-E_B^H. Therefore, the exchange measurements do not prove the existence of conformational exchange and proton hopping between inward-open E_A^--E_B^H and outward-open E_A^--E_B^H. These previous measurements are consistent with the hop-free mechanism.

Using our findings and others reported in the literature, we propose the transport model in Fig. 7 and explain the steps as follows. Step 1: inward-open E_A^H-E_B^H deprotonates at Glu14$_A$ to form E_A^--E_B^H under cytoplasmic pH conditions of *E. coli*. Step 2: drug binds to E_A^--E_B^H, forming E_A^--E_B^H-drug. Step 3: drug binding induces a more acidic pK_a value for Glu14$_B$, favoring formation of E_A^--E_B^--drug (9). Step 4: conformational exchange from inward-open E_A^--E_B^--drug to the outward-open state moves the drug from the cytoplasmic to periplasmic side of the membrane. Step 5: Glu14$_B$ protonates at acidic pH values in the periplasm in *E. coli*, resulting in E_A^--E_B^H-drug. Step 6: drug is released, which occurs at a faster rate for E_A^--E_B^H-drug than E_A^--E_B^--drug (29). Step 7: outward-open E_A^--E_B^H protonates Glu14$_A$ to form E_A^H-E_B^H. Step 8: conformational exchange switches outward-open E_A^H-E_B^H to the inward-open state. The

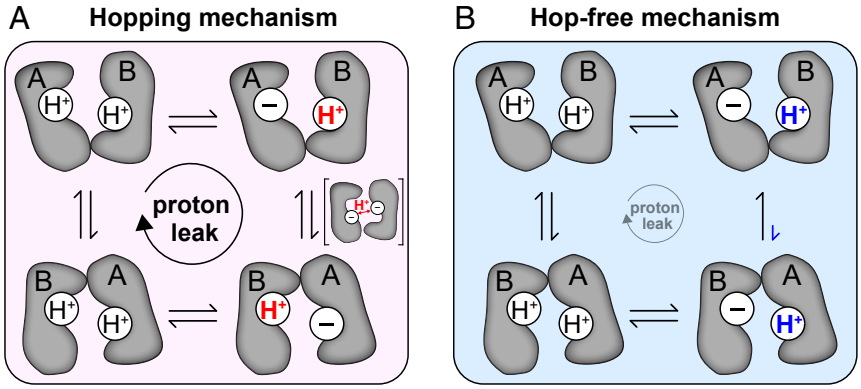

Fig. 6. Conformational exchange mechanisms displaying (*A*) proton hopping and (*B*) no proton hopping. Monomer A or B are indicated within each subunit; "H^+" and "−" correspond to protonated or deprotonated Glu14, respectively. The hopping mechanism leads to significant proton leak, while the hop-free mechanism reduces proton leak.

preferred pathway in this model reduces proton leakage since exchange between E_A^--E_B^H and E_A^H-E_B^- is unfavorable both for the inward-open and outward-open conformations.

In conclusion, we discovered that the asymmetric structure of EmrE and not the presence of electrostatic coupling determines the two pK_a values of Glu14 in the dimer. Thus, in the absence of proton hopping, we propose the energy difference between the two singly proton-bound states (E_A^--E_B^H and E_A^H-E_B^-) reduces the probability of conformational exchange and proton leakage. Since several transporters contain inverted repeat domains and essential anionic residues similar to EmrE (30–32), the hop-free model may explain the lack of proton leakage in other secondary active transporters. The hop-free mechanism can also be considered with the membrane potential, which may further reduce proton leak cycles to conserve energy for uphill transport (33).

Materials and Methods

Protein Expression and Purification. Expression and purification of EmrE was performed as previously reported (8, 16, 17, 34). Briefly, EmrE was expressed as a fusion construct with maltose-binding protein in BL21(DE3) *E. coli* and purified using affinity and size exclusion chromatography in n-dodecyl-β-D-maltopyranoside (DDM, Anatrace). For solid-state NMR experiments, isotopically labeled EmrE was expressed in minimal media (M9) with $^{13}C_6$ glucose and ^{15}N ammonium chloride, while unlabeled EmrE was expressed in LB media. For solution NMR experiments, isotopically enriched EmrE was expressed in M9 media with perdeuterated glucose and ^{15}N ammonium chloride, while unlabeled EmrE was expressed in M9 media with perdeuterated glucose and natural abundance ammonium chloride. EmrE mutants of $EmrE^{E14Q}$, $EmrE^{L51I}$, and $EmrE^{E14Q,\ L51I}$ were constructed using site directed mutagenesis and expressed in the same manner as described above.

NMR Sample Preparation. Preparation of heterodimer samples, EmrE-$EmrE^{L51I}$ or EmrE-$EmrE^{E14Q}$ or EmrE-$EmrE^{E14Q,\ L51I}$, involved mixing an isotopically labeled protein with an unlabeled protein at a ratio of 1/1.6 (mol/mol). The mixture was incubated in DDM and 50 mM DTT for 1 h at 37 °C (19).

For solid-state NMR samples, EmrE was reconstituted into 1,2-di-*O*-tetradecyl-sn-glycero-3-phosphocholine (*O*-14:0-PC) (Avanti Polar Lipids) at a lipid to protein ratio of 30/1 (mol/mol). DDM detergent was removed by addition of Bio-Beads SM-2 resin (Bio-Rad) in a 100-fold excess relative to DDM (wt/wt). Proteoliposomes in 150 mM sodium phosphate and 20 mM sodium chloride were ultracentrifuged for 12 h at 436,000 × *g* using a TLA-100 rotor (Beckman-Coulter). The proteoliposome pellet was packed into a 3.2 mm MAS rotor using sample spacers to prevent dehydration. To change the pH, the samples were buffer exchanged by resuspending proteoliposomes at pH 5.0, 8.0, or 10.0, performing freeze-thaw cycles, and ultracentrifuging.

For solution NMR samples, EmrE was reconstituted into DMPC/DHPC with the perdeuterated chains (14:0 PC D54 and 6:0 PC D22, Cortecnet) to make isotropic bicelles (q = 0.33). The DMPC lipid to protein ratio was 30/1 (mol/mol). The final heterodimer samples contained 1.39 mM total protein and homodimer sample contained 0.533 mM protein. The solution NMR buffer was 150 mM sodium phosphate, 20 mM sodium chloride, and 10% deuterium oxide.

Solid-State NMR Spectroscopy. Solid-state NMR spectra were recorded on an Agilent DD2 NMR spectrometer operating at a ^1H frequency of 600 MHz (14.1 T) equipped with a 3.2 mm triple resonance MAS probe manufactured by Black Fox, LLC. The sample temperature was set to −20 °C or −5 °C with an MAS rate at 8,333 ± 5 Hz or 12,500 ± 5 Hz. Typical 90° pulse lengths of ^1H, ^{13}C, and ^{15}N nuclei were 2.5, 4.5, and 5 μs, respectively. ^1H-^{13}C/^{15}N

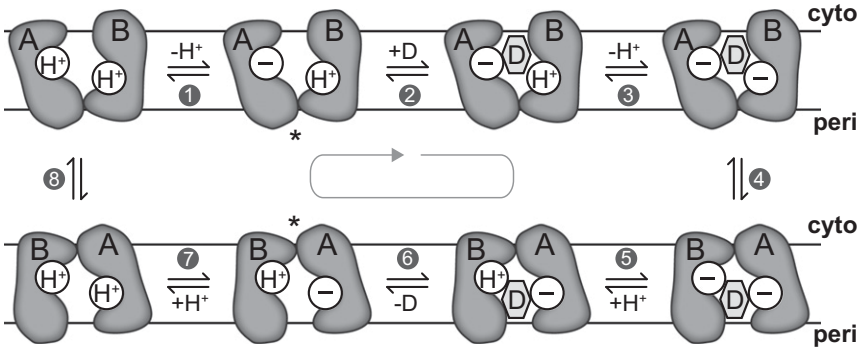

Fig. 7. Model of proton-coupled drug efflux by EmrE. Monomer A or B are indicated and "H^+" or "−" within each monomer correspond to protonated or deprotonated Glu14, respectively; the drug is indicated with a "D." The equilibria are indicated by numbers and are referenced in the text. Asterisks correspond to the E_A^--E_B^H inward-open (*top*) and outward-open conformations (*bottom*); exchange between these conformations results in a proton leak cycle (Figure 6*A*) and is disallowed for efficient exchange.

cross-polarization used radiofrequency (RF) pulses of 55.6 (or 50 kHz) for ^{13}C (or ^{15}N) with a tangent ramp (35) on ^{1}H. Frequency selective polarization transfers from ^{15}N to ^{13}CA were carried out using SPECIFIC-CP (36) with a 5.5 ms tangent ramp on ^{13}C and with RF amplitudes of ~18.8, ~31.3, and 110 kHz on ^{15}N, ^{13}C, and ^{1}H, respectively. The ^{1}H RF power was set to 100 kHz for decoupling during acquisition and evolution periods.

For DQSQ experiments, an SPC-5 pulse (37) with 1.2 ms Z-filtered time was used for the conversion and reconversion steps. During the SPC-5 element, continuous wave ^{1}H decoupling with an RF amplitude of 100 kHz was used. REDOR dephasing of ^{15}N in the DQSQ-REDOR experiment was achieved by a composite 90°-180°-90° pulse train (38) using a 5 μs 90° pulse. The chemical shifts of ^{13}C and ^{15}N were indirectly calibrated by external referencing the CH_2 resonance of adamantane to 40.48 ppm (39). All the multidimensional NMR spectra were processed in NMRPipe (40) and analyzed using Sparky (41).

Solution NMR Spectroscopy. Solution NMR spectra were acquired at 37 °C on a Bruker spectrometer operating at a ^{1}H frequency of 600 MHz (14.1 T) equipped with a triple resonance TCI cryogenic probe. For pH titrations, 2D $^{1}H/^{15}N$ TROSY experiments were recorded with spectral widths of 12,019.2 Hz and 1,520.6 Hz for ^{1}H and ^{15}N, respectively. The acquisition (^{1}H) and evolution times (^{15}N) were 59.9 ms and 22.8 ms. The pH stability of NMR samples was monitored before and after each TROSY experiment; the pH fluctuated by ±0.02. The total experimental time was ~1.5 d to complete the full pH titration curve. Residues with significant chemical shift perturbations, defined as $^{1}H > 0.03$ ppm and $^{15}N > 0.3$ ppm, were fitted in a global manner using a macroscopic two-pK_a model (Eq. **1**) (42) or a one-pK_a model (Eq. **2**).

$$\delta = \frac{\delta_{H_2A} + \delta_{HA}10^{pH-pK_{a,1}} + \delta_A 10^{[2pH-(pK_{a,1}+pK_{a,2})]}}{1 + 10^{(pH-pK_{a,1})+} 10^{[2pH-(pK_{a,1}+pK_{a,2})]}} \quad [1]$$

$$\delta = \frac{\delta_{HA} + \delta_A 10^{pH-pK_a}}{1 + 10^{pH-pK_a}} \quad [2]$$

δ_{H_2A}, δ_{HA}, and δ_A are the chemical shifts of the fully protonated, half-protonated. and deprotonated states, respectively, in Eq. **1**. δ is the observed chemical shift. δ_{HA} and δ_A are the chemical shifts of the protonated and deprotonated states, respectively, in Eq. **2**.

Quantification of Free Energies from Heterodimer Samples. Determination of populations, equilibrium constants, and free energies for EmrE heterodimers have been described previously (19). In brief, the equilibrium for wild-type EmrE in a heterodimer with a mutant is given in Eq. **3**, where subscripts refer to monomer A or B in the dimer:

$$WT_A \cdot mutant_B \rightleftharpoons mutant_A \cdot WT_B. \quad [3]$$

Populations of wild-type EmrE occupying monomer A (p_A) or monomer B (p_B) in the heterodimer are calculated using Eq. **4**:

$$\frac{I_{A,obs}}{I_{B,obs}} = \frac{I_A}{I_B} \frac{(f_{homo} + f_{het} \quad p_A)}{(f_{homo} + f_{het} \quad p_B)}. \quad [4]$$

$I_{A,obs}$ and $I_{B,obs}$ are the observed ratio of intensities of monomer A and B peaks in a heterodimer spectrum, respectively. I_A and I_B are the intensities of monomer A and B peaks from a homodimer reference spectrum, which is needed since A and B peaks are not intrinsically the same. f_{homo} and f_{het} is the fraction of homodimers and heterodimers formed by the isotopically labeled protein in preparation of the heterodimer samples; f_{homo} and f_{het} were 0.24 and 0.76, respectively, by assuming statistical mixing of the 1/1.6 molar ratio of isotopically labeled and unlabeled proteins. Addition of p_A and p_B is equal to 1, and their ratio gives the equilibrium constant. The free energies reported are calculated from the equilibrium constant.

$I_{A,obs}$ and $I_{B,obs}$ were measured for resolved isoleucine methyl peaks ($-^{13}C^{\delta}H_3$) in heteronuclear multiple quantum coherence spectra corresponding to the isotopically enriched protein in the heterodimer: Ile11, Ile54, Ile58, Ile62, Ile68, Ile88, and Ile101 for EmrE-EmrE^{L51I}; Ile62, Ile68, Ile88, and Ile100 for EmrE-EmrE^{E14Q}; Ile16, Ile54, Ile58, and Ile101 for EmrE-EmrE$^{E14Q,\ L51I}$. I_A and I_B were measured for the same isoleucine methyl peaks of wild-type EmrE. The free energy of the conformational preference of EmrE-EmrE^{E14Q} heterodimers at a pH value of 6.2 was estimated as the difference in the free energy of EmrE-EmrE$^{E14Q,\ L51I}$ and EmrE-EmrE^{L51I}. This value of ~0.6 kcal/mol at pH 6.2 was subtracted from the free energy of the conformational preference of EmrE-EmrE^{E14Q} heterodimers at pH 9.5 (~3.5 kcal/mol) to give the intrinsic free energy difference between E_A^--E_B^H and E_A^H-E_B^- (~2.9 kcal/mol).

Data Availability. All study data are included in the article and/or *SI Appendix*.

ACKNOWLEDGMENTS. This work was supported by NIH (R01 AI108889) and NSF awards (MCB 1506420) to N.J.T. NMR data were collected using a cryoprobe that was supported by an NIH S10 grant (OD016343). We thank M. (Leninger) Crames for helpful discussions.

1. J. M. A. Blair, M. A. Webber, A. J. Baylay, D. O. Ogbolu, L. J. V. Piddock, Molecular mechanisms of antibiotic resistance. *Nat. Rev. Microbiol.* **13**, 42–51 (2015).
2. M. Saleh, D. C. Bay, R. J. Turner, Few conserved amino acids in the small multidrug resistance transporter EmrE influence drug polyselectivity. *Antimicrob. Agents Chemother.* **62**, e00461-18 (2018).
3. S. Schuldiner, EmrE, a model for studying evolution and mechanism of ion-coupled transporters. *Biochim. Biophys. Acta* **1794**, 748–762 (2009).
4. C. W. Sikora, R. J. Turner, Investigation of ligand binding to the multidrug resistance protein EmrE by isothermal titration calorimetry. *Biophys. J.* **88**, 475–482 (2005).
5. D. Rotem, S. Schuldiner, EmrE, a multidrug transporter from *Escherichia coli*, transports monovalent and divalent substrates with the same stoichiometry. *J. Biol. Chem.* **279**, 48787–48793 (2004).
6. H. Yerushalmi, M. Lebendiker, S. Schuldiner, EmrE, an *Escherichia coli* 12-kDa multidrug transporter, exchanges toxic cations and H+ and is soluble in organic solvents. *J. Biol. Chem.* **270**, 6856–6863 (1995).
7. E. A. Morrison *et al*., Antiparallel EmrE exports drugs by exchanging between asymmetric structures. *Nature* **481**, 45–50 (2011).
8. A. Gayen, M. Leninger, N. J. Traaseth, Protonation of a glutamate residue modulates the dynamics of the drug transporter EmrE. *Nat. Chem. Biol.* **12**, 141–145 (2016).
9. A. E. Robinson, N. E. Thomas, E. A. Morrison, B. M. Balthazor, K. A. Henzler-Wildman, New free-exchange model of EmrE transport. *Proc. Natl. Acad. Sci. U.S.A.* **114**, E10083–E10091 (2017).
10. D. Rotem, S. Steiner-Mordoch, S. Schuldiner, Identification of tyrosine residues critical for the function of an ion-coupled multidrug transporter. *J. Biol. Chem.* **281**, 18715–18722 (2006).
11. Y. Elbaz, N. Tayer, E. Steinfels, S. Steiner-Mordoch, S. Schuldiner, Substrate-induced tryptophan fluorescence changes in EmrE, the smallest ion-coupled multidrug transporter. *Biochemistry* **44**, 7369–7377 (2005).
12. G. Platzer, M. Okon, L. P. McIntosh, pH-dependent random coil (1)H, (13)C, and (15)N chemical shifts of the ionizable amino acids: a guide for protein pK a measurements. *J. Biomol. NMR* **60**, 109–129 (2014).
13. J. Li, A. Sae Her, N. J. Traaseth, Site-specific resolution of anionic residues in proteins using solid-state NMR spectroscopy. *J. Biomol. NMR* **74**, 355–363 (2020).
14. K. Schmidt-Rohr, K. J. Fritzsching, S. Y. Liao, M. Hong, Spectral editing of two-dimensional magic-angle-spinning solid-state NMR spectra for protein resonance assignment and structure determination. *J. Biomol. NMR* **54**, 343–353 (2012).
15. Y. J. Chen *et al*., X-ray structure of EmrE supports dual topology model. *Proc. Natl. Acad. Sci. U.S.A.* **104**, 18999–19004 (2007).
16. A. Gayen, J. R. Banigan, N. J. Traaseth, Ligand-induced conformational changes of the multidrug resistance transporter EmrE probed by oriented solid-state NMR spectroscopy. *Angew. Chem. Int. Ed. Engl.* **52**, 10321–10324 (2013).
17. M. K. Cho, A. Gayen, J. R. Banigan, M. Leninger, N. J. Traaseth, Intrinsic conformational plasticity of native EmrE provides a pathway for multidrug resistance. *J. Am. Chem. Soc.* **136**, 8072–8080 (2014).
18. N. J. B. Traaseth, J. R. Banigan, M. Leninger, Exploring transporters within the SMR family using solid-state NMR spectroscopy. *eMagRes* **4**, 551–559 (2015).
19. M. Leninger, A. Sae Her, N. J. Traaseth, Inducing conformational preference of the membrane protein transporter EmrE through conservative mutations. *eLife* **8**, e48909 (2019).
20. R. Dastvan, A. W. Fischer, S. Mishra, J. Meiler, H. S. Mchaourab, Protonation-dependent conformational dynamics of the multidrug transporter EmrE. *Proc. Natl. Acad. Sci. U.S.A.* **113**, 1220–1225 (2016).
21. E. A. Morrison, A. E. Robinson, Y. Liu, K. A. Henzler-Wildman, Asymmetric protonation of EmrE. *J. Gen. Physiol.* **146**, 445–461 (2015).
22. J. V. Vermaas, S. B. Rempe, E. Tajkhorshid, Electrostatic lock in the transport cycle of the multidrug resistance transporter EmrE. *Proc. Natl. Acad. Sci. U.S.A.* **115**, E7502–E7511 (2018).
23. V. Ovchinnikov, T. A. Stone, C. M. Deber, M. Karplus, Structure of the *EmrE* multidrug transporter and its use for inhibitor peptide design. *Proc. Natl. Acad. Sci. U.S.A.* **115**, E7932–E7941 (2018).
24. S. Kumar, R. Nussinov, Close-range electrostatic interactions in proteins. *ChemBioChem* **3**, 604–617 (2002).
25. H. X. Zhou, X. Pang, Electrostatic interactions in protein structure, folding, binding, and condensation. *Chem. Rev.* **118**, 1691–1741 (2018).
26. H. Yerushalmi, S. Schuldiner, An essential glutamyl residue in EmrE, a multidrug antiporter from *Escherichia coli*. *J. Biol. Chem.* **275**, 5264–5269 (2000).
27. A. A. Kermani, C. B. Macdonald, R. Gundepudi, R. B. Stockbridge, Guanidinium export is the primal function of SMR family transporters. *Proc. Natl. Acad. Sci. U.S.A.* **115**, 3060–3065 (2018).
28. M. Rapp, S. Seppälä, E. Granseth, G. von Heijne, Emulating membrane protein evolution by rational design. *Science* **315**, 1282–1284 (2007).

29. Y. Adam, N. Tayer, D. Rotem, G. Schreiber, S. Schuldiner, The fast release of sticky protons: Kinetics of substrate binding and proton release in a multidrug transporter. *Proc. Natl. Acad. Sci. U.S.A.* **104**, 17989–17994 (2007).
30. O. Pornillos, G. Chang, Inverted repeat domains in membrane proteins. *FEBS Lett.* **580**, 358–362 (2006).
31. O. Boudker, G. Verdon, Structural perspectives on secondary active transporters. *Trends Pharmacol. Sci.* **31**, 418–426 (2010).
32. D. Du *et al*., Multidrug efflux pumps: Structure, function and regulation. *Nat. Rev. Microbiol.* **16**, 523–539 (2018).
33. X. C. Zhang, M. Liu, G. Lu, J. Heng, Thermodynamic secrets of multidrug resistance: A new take on transport mechanisms of secondary active antiporters. *Protein Sci.* **27**, 595–613 (2018).
34. J. R. Banigan, A. Gayen, M. K. Cho, N. J. Traaseth, A structured loop modulates coupling between the substrate-binding and dimerization domains in the multidrug resistance transporter EmrE. *J. Biol. Chem.* **290**, 805–814 (2015).
35. M. Baldus, D. G. Geurts, S. Hediger, B. H. Meier, Efficient N-15-C-13 polarization transfer by adiabatic-passage Hartmann-Hahn cross polarization. *J. Magn. Reson. A* **118**, 140–144 (1996).
36. M. Baldus, A. T. Petkova, J. H. Herzfeld, R. G. Griffin, Cross polarization in the tilted frame: Assignment and spectral simplification in heteronuclear spin systems. *Mol. Phys.* **95**, 1197–1207 (1998).
37. M. Hohwy, C. M. Rienstra, C. P. Jaroniec, R. G. Griffin, Fivefold symmetric homonuclear dipolar recoupling in rotating solids: Application to double quantum spectroscopy. *J. Chem. Phys.* **110**, 7983–7992 (1999).
38. M. H. Levitt, R. Freeman, Nmr population-inversion using a composite pulse. *J. Magn. Reson.* **33**, 473–476 (1979).
39. C. R. Morcombe, K. W. Zilm, Chemical shift referencing in MAS solid state NMR. *J. Magn. Reson.* **162**, 479–486 (2003).
40. F. Delaglio *et al*., NMRPipe: A multidimensional spectral processing system based on UNIX pipes. *J. Biomol. NMR* **6**, 277–293 (1995).
41. T. D. Goddard, D. G. Kneller, *SPARKY 3* (University of California, San Francisco).
42. L. P. McIntosh *et al*., Dissecting electrostatic interactions in *Bacillus circulans* xylanase through NMR-monitored pH titrations. *J. Biomolec. NMR* **51**, 5–19 (2011).